Jurnal Teknologi

Full Paper

SUPPRESSION OF SOMMERFELD EFFECT IN POWER TRANSMISSION SYSTEM EMPLOYING CARDAN SHAFT THROUGH PHASE ANGLE ARRANGEMENT

Mohd Hazri Omar[a]*, Muhajir Ab Rahim[b], Mohd Noor Arib Md Rejab[a], Muhamad Norhisham Abdul Rani[c]

[a]Faculty of Mechanical Engineering and Technology, UNIMAP, 02600, Arau, Perlis, Malaysia
[b]Faculty of Electrical Engineering and Technology, UNIMAP, 02600, Arau, Perlis, Malaysia
[c]School of Mechanical Engineering, Universiti Teknologi MARA (UiTM), 40450 Shah Alam, Selangor, Malaysia

Article history
Received
5 September 2023
Received in revised form
26 November 2023
Accepted
15 January 2024
Published Online
23 June 2024

*Corresponding author
mohdhazri@ptss.edu.my

Graphical abstract

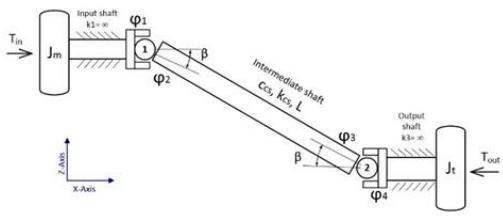

Abstract

In a power transmission system with a cardan shaft, the Sommerfeld effect occurs, which is characterized by speed capture and release at the resonance range. Suppression of the Sommerfeld effect is critical for smooth and reliable operation. This study aims to suppress the Sommerfeld effect in a transmission system by compensating the phase angle between the two universal joints installed in the cardan shaft. The differential equations of motion representing the dynamics of the system are derived using the Lagrange equation. The responses are simulated numerically using the Runge–Kutta algorithm for scenarios with constant and gradually varying input torque. To suppress the Sommerfeld effect, the phase angle is set to 25%, 50%, 75% and 100% of the maximum twist angle observed in the subcritical speed range of the in-phase configuration. With the phase angle of 25%, the Sommerfeld effect is damped, where the output speed only deviates by 5% from the estimated value for both input torque scenarios. It is shown how the change of the phase angle attenuates the Sommerfeld effect and the system vibrations, which should be considered in the development and practical implementation.

Keywords: Power transmission system, cardan shaft, speed capture, phase angle, universal joint

Abstrak

Dalam sistem penghantaran kuasa dengan aci cardan, kesan Sommerfeld berlaku, yang dicirikan oleh tangkapan dan pelepasan kelajuan pada julat resonans.. Melemahkan kesan Sommerfeld adalah penting untuk operasi yang lancar dan boleh dipercayai. Kajian ini bertujuan untuk melemahkan kesan Sommerfeld dalam sistem penghantaran dengan mengimbangi sudut fasa antara dua sendi universal yang dipasang dalam aci cardan. Persamaan pembezaan gerakan yang mewakili dinamik sistem diterbitkan menggunakan persamaan Lagrange. Respons disimulasikan secara berangka menggunakan algoritma Runge-Kutta untuk senario dengan daya kilas

masukan yang malar dan berubah-ubah secara beransur-ansur. Untuk melemahkan kesan Sommerfeld, sudut fasa ditetapkan kepada 25%, 50%, 75% dan 100% daripada sudut kilasan maksimum yang diperhatikan dalam julat kelajuan subkritikal konfigurasi dalam fasa. Dengan sudut fasa ialah 25%, kesan Sommerfeld dilemahkan, di mana kelajuan output hanya menyimpang sebanyak 5% daripada nilai anggaran untuk kedua-dua senario daya kilas masukan. Ia ditunjukkan bagaimana perubahan sudut fasa melemahkan kesan Sommerfeld dan getaran sistem, yang harus dipertimbangkan dalam pembangunan dan pelaksanaan praktikal.

Kata kunci: Sistem penghantaran kuasa, aci cardan, tangkapan kelajuan, sudut fasa, sendi universal

1.0 INTRODUCTION

The cardan shaft is an essential part of a mechanical power transmission system that transmits torque between two non-collinear shafts, compensating for angular misalignment. It has universal joints at both ends to compensate for misalignment between the driving and driven sides. One of the main advantages of the cardan shaft is its ability to efficiently transmit torque between non-collinear shafts [1, 2]. The transmission system can effectively compensate for angular misalignment by using a cardan shaft, so that the input and output shafts maintain a constant speed ratio. The cardan shaft is commonly used in automotive drivetrain systems, especially rear-wheel drive and all-wheel drive vehicles. The cardan shaft is also used in various industrial machines such as mining machines [3], railway industry [4] and marine propulsion systems [5] where misaligned shaft arrangements are required. It is reported that the use of a cardan shaft in mechanical systems causes problems with vibrations due to the kinematics of the cardan joint[6, 7]. These vibrations cause fluctuating loads on the supporting bearings, coupling components and surrounding structures, resulting in increased stress, wear and lower system efficiency [8–10] *et al.*

One of the main causes of vibration in transmission systems with cardan shafts is the degree of angular misalignment that the universal joints exhibit [11, 12]. As the angular misalignment increases, the cardan shaft vibrations increase. In addition to the presence of angular misalignment, the phasing of the universal joint yokes, which are located at both ends of the cardan shaft, also has a significant effect on the vibration characteristics of the transmission system. Most previous research has focused on the analysis of systems with in-phase configurations. However, there are few studies on the vibrations caused by systems with out-of-phase configuration. An and Wang [13] investigated the kinematic relationship of a transmission system with a cardan shaft, focusing on the effects of unequal angular misalignments and non-zero phase angles. The results show that output speed variations worsen when these two conditions coincide. Fischer and Paul [14] conducted an experimental study that showed that the variation can be cancelled if both joints have the same angular displacement by ensuring that the phase angle is equal to the twist angle. Wu *et al*. [15] demonstrated that a suitable phase angle configuration within a multi-universal joint system can mitigate torsional vibrations and should be considered in the design of drive shafts.

The Sommerfeld effect is a type of instability that often occurs in non-ideal systems with limited power supply and can be identified by the speed capture and release at critical speed [16]. As a result, the system is unable to rotate smoothly and is trapped in resonance for a considerable time. During speed capture, most of the power source is used to vibrate the structure instead of increasing the speed of rotation. When the power supply exceeds a particular threshold, the system can escape from speed capture, which is characterized by a sudden increase in rotational speed followed by a sudden decrease in vibration amplitudes. Due to torsional vibrations in the cardan shaft, the Sommerfeld effect can significantly affect the performance and reliability of the driveline. According to Bharti and Samantaray [17], the Sommerfeld effect in the driveline system can be attributed to torsional vibrations resulting from the angular misalignment of the universal joint. In the study, two distinct regions were observed where the phenomenon of speed capture and escape occurred. One region was close to half of the natural frequency, while the other region was observed at the natural frequency. These regions were classified as subcritical and critical speed regions, respectively. They suggested that reducing the angular misalignments or increasing the torsional damping of the shaft could reduce the amplitude of vibration and prevent Sommerfeld effects. Yao and DeSmidt [18] evaluated the Sommerfeld effect caused by the coupled torsional and lateral vibrations of the driveline. The study investigated the vibrations under different conditions of static angular displacement and lateral damping, restricting the observation of the Sommerfeld effect to the subcritical velocity range. They concluded that the speed capture

phenomenon is primarily associated with the torsional mode. Therefore, the Sommerfeld effect has the potential to affect the performance and reliability of a rotor system and lead to increased vibration amplitudes that can cause damage or failure of the system [19]. Reducing this effect is therefore crucial for the smooth operation of rotors and provides a more robust transmission system.

The suppression of the Sommerfeld effect is a topic that plays a major role in research and technology in the field of rotor dynamics. Over the years, researchers have explored various approaches to mitigate or suppress the Sommerfeld effect with the aim of improving the stability and reliability of rotor systems. The Sommerfeld effect can be suppressed by modulating the dynamic parameters of the system, changing the drive source or using passive, active and semi-active control strategies [20]. The study by Bharti *et al*. [21] provided evidence that the interaction between the DC motor and the whirling rotor in a non-ideal system can lead to stability within speed ranges that would be unstable in an ideal system. A common approach to suppress the Sommerfeld effect is to introduce auxiliary damping mechanisms. These mechanisms are designed to dissipate energy from the rotor system, reducing the potential for self-excited vibrations. Examples of auxiliary damping mechanisms include the use of friction dampers, eddy current dampers and tuned mass dampers. These devices introduce additional energy dissipation mechanisms to counteract the destabilizing forces caused by the Sommerfeld effect. Jha and Dasgupta [22] used fractional order parameters in the external damping term to suppress the Sommerfeld effect in an internally damped DC motor-driven discrete rotor system. Active control strategies to suppress the Sommerfeld effect have also been explored. Active control strategies have shown promising results in suppressing vortex mode instability, especially for complex rotor systems with changing operating conditions. Jha and Dasgupta [23] employed linearized active magnetic bearings to mitigate the Sommerfeld effect of an internally damped unbalanced flexible shaft-disc system. In addition, the use of smart materials has emerged as a potential way to suppress the Sommerfeld effect. Smart materials, such as magnetorheological fluids or piezoelectric materials, can have controllable properties that can be used to improve the stability of rotor systems. By incorporating these materials into the design of rotors or bearings, the dynamics of the system can be changed and self-excited vibrations can be actively suppressed.

The suppression of the Sommerfeld effect in rotor systems has attracted a lot of attention from researchers and engineers. Significant progress has been made in mitigating the Sommerfeld effect through various techniques such as optimisation of bearings, additional damping mechanisms, active control strategies and the use of smart materials. However, further studies and developments are needed to address the specific requirements and limitations of different rotor systems in real applications. Therefore, a comprehensive analysis that takes into account the change in system geometry is essential for the development of a practical suppression approach. This study aims to suppress the Sommerfeld effect in a cardan shaft transmission system by compensating for the phasing of the cardan shaft yokes. The governing equations representing the dynamics of the system with the phase angle are derived using the Lagrange formulation. The numerical simulation is performed in scenarios with constant and gradually varying input torque. The output speed and the twist angle are the main indicators simulated using the Runge-Kutta algorithm. This study is based exclusively on numerical simulations of the mathematical model.

2.0 SYSTEM DESCRIPTION AND GOVERNING EQUATIONS

A typical mechanical power transmission system consists of driving and driven components, a cardan shaft and other rotating parts. The cardan shaft is used when the axes of the driving and driven components are not properly aligned, mainly to compensate for different relative angles between the drive and driven shafts. Figure 1 shows a schematic diagram of the power transmission system using a cardan shaft. The cardan shaft is connected to drive and driven shafts with an angular misalignment, β. The length of the cardan shaft is denoted as L, while its outer diameter is represented by d_{out}. The variable J_m denotes the cumulative rotational inertia of the input shaft and all additional rotating elements on the driving side. The output shaft carries a rotor disk with a lumped moment of inertia of J_t. For the system under consideration, the angular positions of the shaft ends are denoted by φ_1, φ_2, φ_3 , and φ_4. The torque applied to the drive side and driven side is represented by T_{in} and T_{out}, respectively. The cardan shaft has a torsional stiffness, k_{cs}, and torsional damping, c_{cs} is attached to the input and output shafts. The damping of the system is modeled as $c_{cs} = \xi_{cs} k_{cs}$, where ξ_{cs} is the viscous damping coefficient. The following assumptions are made when modelling the power transmission system. Firstly, the input and output shafts are considered as rigid shafts. Secondly, the lateral vibrations of the system are eliminated by a support bearing [24, 25]. Thirdly, the angular misalignment for both universal joints is kept at an equal value.

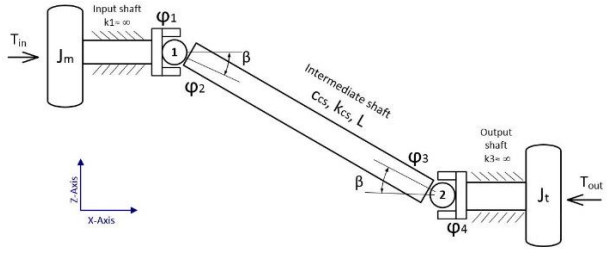

Figure 1 Schematic of the dynamic model of the driveline

From the well-known kinematic relationship of universal joint, the angular positions of the yokes on the driving, φ_2 and driven sides, φ_3 of a cardan shaft can be expressed as [25, 26]

$$tan(\varphi_2) = \frac{tan(\varphi_1)}{cos(\beta)} \quad (1)$$

$$tan(\varphi_3) = \frac{tan(\varphi_4)}{cos(\beta)} \quad (2)$$

Equations 1 and 2 show that with an increase in angular misalignment, the variation in angular positions for both yokes increase. In addition to the angular misalignment, the variation in angular position is also influenced by the phasing of the two yokes. The cardan shaft has an in-phase configuration when the yokes of the two universal joints are aligned in the same plane. If the yoke on the driven side of the cardan shaft is shifted by the phase angle a, the cardan shaft is said to have an out-of-phase configuration. The aim of this study is to investigate the potential of the phase angle in suppressing the Sommerfeld effect. The phase angle is thus shifted in the same direction as the input rotational motion by shifting the yoke on the driven side of the cardan shaft to an angular position of φ_{3S}, as shown in Figure 2.

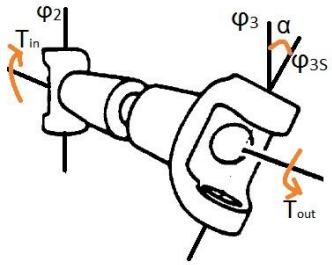

Figure 2 Phase angle between the two universal joint yokes

Thus, Equation 2 is rewritten with the presence of phase angle as [13]

$$tan(\varphi_3 + \alpha) = \frac{tan(\varphi_4 + \delta)}{cos(\beta)} \quad (3)$$

The symbol δ is used to denote the angular displacement of the output shaft's yoke, which is determined by the following calculation [26].

$$tan(\delta) = tan(\alpha)\, cos(\beta) \quad (4)$$

Subsequently, the differentiation of Equations 1 and 3 with respect to time yields the correlation between the angular speeds at the driving and driven sides of the cardan shaft, denoted as [27].

$$\dot{\varphi}_2 = \dot{\varphi}_i \frac{cos(\beta)}{1 - sin^2(\beta)\, cos^2(\varphi_1)} \quad (5)$$

$$\dot{\varphi}_3 = \dot{\varphi}_4 \frac{cos(\beta)}{1 - sin^2(\beta)\, cos^2(\varphi_4 + \delta)} \quad (6)$$

The system equations of motion are derived by using Lagrange's equations.

$$\frac{d}{dt}\left(\frac{\partial K}{\partial \dot{q}_i}\right) - \frac{\partial K}{\partial q_i} + \frac{\partial D}{\partial \dot{q}_i} + \frac{\partial P}{\partial q_i} = Q_i, i = 1,2,.,n \quad (7)$$

with the generalised coordinate of the system representing the input speed, $\dot{\varphi}_1$ and the output speed, $\dot{\varphi}_4$ is described as

$$q = \{\dot{\varphi}_1 \quad \dot{\varphi}_4\}^T \quad (8)$$

The kinetic energy is expressed as

$$K = \frac{1}{2} J_m \dot{\varphi}_1{}^2 + \frac{1}{2} J_t \dot{\varphi}_4{}^2 \quad (9)$$

The damping dissipated energy is expressed as

$$D = \frac{1}{2} c_{cs} (\dot{\varphi}_2 - \dot{\varphi}_3)^2 \quad (10)$$

From Equations 5 and 6, Equation 10 is expressed as

$$D = \frac{1}{2} c_{cs} \left(\dot{\varphi}_i \frac{cos(\beta)}{1 - sin^2(\beta)\, cos^2(\varphi_1)} - \dot{\varphi}_4 \frac{cos(\beta)}{1 - sin^2(\beta)\, cos^2(\varphi_4 + \delta)} \right)^2 \quad (11)$$

The potential energy is expressed as

$$P = \frac{1}{2} k_{cs} (\varphi_2 - \varphi_3)^2 \quad (12)$$

Then, the following equations of motion are obtained by substituting Equations 9, 11, and 12 into Equation 7 [28]. After some arrangement, the rotational motion is expressed as

$$J_m \ddot{\varphi}_1 + c_{cs}\eta_{u1}(\eta_{u1}\dot{\varphi}_1 - \eta_{u2}\dot{\varphi}_4) + k_{cs}\eta_{u1}(\varphi_2 - \varphi_3) = T_{in} \quad (13)$$

$$J_t \ddot{\varphi}_4 - c_{cs}\eta_{u2}(\eta_{u1}\dot{\varphi}_1 - \eta_{u2}\dot{\varphi}_4) - k_{cs}\eta_{u2}(\varphi_2 - \varphi_3) = -T_{out} \quad (14)$$

where

$$\eta_{u1} = \frac{cos(\beta)}{1 - sin^2(\beta)\, cos^2(\varphi_1)}$$

$$\eta_{u2} = \frac{cos(\beta)}{1 - sin^2(\beta)\, cos^2(\varphi_4 + \delta)} \quad (15)$$

The phenomenon of the angle of twist results from the angular deformation between two points located at the opposite ends of the cardan shaft and is expressed as [29].

$$\theta_{cs} = \varphi_2 - \varphi_3 \tag{16}$$

In accordance with Bharti and Samantaray [17] and Yao and DeSmidt [18], the load on the driven side, T_{out} is simulated by a torsional load viscous resistance coefficient R_{out} and expressed as

$$T_{out} = R_{out}\dot{\varphi}_4 \tag{17}$$

From Equations 16 and 17, Equations 13 and 14 are expressed as

$$J_m\ddot{\varphi}_1 + c_{cs}\eta_{u1}(\eta_1\dot{\varphi}_{u1} - \eta_{u2}\dot{\varphi}_4) + k_{cs}\eta_{u1}(\theta_{cs}) = T_{in} \tag{18}$$

$$J_t\ddot{\varphi}_4 - c_{cs}\eta_{u2}(\eta_{u1}\dot{\varphi}_1 - \eta_{u2}\dot{\varphi}_4) - k_{cs}\eta_{u2}(\theta_{cs}) = -R_{out}\dot{\varphi}_4 \tag{19}$$

Differentiating Equation 16 with respect to time and applying Equations 5 and 6 yield

$$\dot{\theta}_{cs} = \eta_{u1}\dot{\varphi}_1 - \eta_{u2}\dot{\varphi}_4 \tag{20}$$

Subsequently, Equations 18 to 20 are rearranged into a system of five first-order ordinary differential equations, which serve as the basis for carrying out numerical simulations

$$\dot{X}_1 = X_2$$

$$\dot{X}_2 = [T_{in} - c_{cs}\eta_{u1A}(\eta_{u1A}X_2 - \eta_{u2A}X_4) - k_{cs}\eta_{u1A}(X_5)]/J_m$$

$$\dot{X}_3 = X_4$$

$$\dot{X}_4 = \ddot{\varphi}_4 = [-R_{out}X_4 + c_{cs}\eta_2(\eta_{1A}X_2 - \eta_{2A}X_4) + k_{cs}\eta_2(X_5)]/J_t$$

$$\dot{X}_5 = \eta_{u1A}X_2 - \eta_{u2A}X_4 \tag{21}$$

where

$$[X_1 \quad X_2 \quad X_3 \quad X_4 \quad X_5]^T = [\varphi_1 \quad \dot{\varphi}_1 \quad \varphi_4 \quad \dot{\varphi}_4 \quad \theta_{cs}]^T$$

$$\eta_{u1A} = \frac{cos(\beta)}{1 - sin^2(\beta)\,cos^2(X_1)}$$

$$\dot{X}_3 = X_4$$

$$\eta_{u2A} = \frac{cos(\beta)}{1 - sin^2(\beta)\,cos^2(X_3 + \delta)} \tag{22}$$

Responses of the system are obtained by numerically solving Equation 21 using the Runge-Kutta algorithm in MATLAB. The parameter values used for the numerical solution are taken from Bharti and Samantaray [17] as shown in Table 1. In this study, the effects of phase angle on Sommerfeld effect are investigated with constant and gradually changing input torque. The simulation is started with an in-phase configuration. Then the phase angle is reconfigured using the maximum twist when operating at subcritical speed.

Table 1 Parameter values of the power transmission system

Parameters Description	Symbol	Value	Unit
Moment of inertia of the drive side	J_m	0.2	kg.m^2
Moment of inertia of the driven side	J_t	2.8	kg.m^2
Outer diameter of the intermediate shaft	d_{out}	0.05	m
Length of the intermediate shaft	L	5	m
Torsional stiffness of the intermediate shaft	k_{cs}	5796	Nm.rad^{-1}
Torsional damping coefficient of the intermediate shaft	ξ_{cs}	0.002	s
Load damping on the driven side	R_{out}	3	Nms/rad
Angular misalignment	β	1	rad

3.0 RESULTS AND DISCUSSION

This section presents the results obtained by solving Equation 21 numerically. The Runga-Kutta algorithm is used to calculate the angle of twist and output speed based on the predetermined parameters listed in Table 1. In this system, the output speed is expected to be more uniform compared to the input speed due to the higher moment of inertia. Without torsional vibrations, the estimated output speed can be calculated as $\overline{\varphi}_{out} = T_{in}/R_{out}$. As reported in previous studies [17, 18], the natural frequency is important because of its correlation with the Sommerfeld effect. The Sommerfeld effect occurs when an average output speed approaches the natural frequency or one of its even fractions. Based on the given parameters, the natural frequency of the system is 176 rad/s when the misalignment angle is zero. In this study, the influence of the phase angle on the suppression of the Sommerfeld effect is investigated in

scenarios with constant and gradually varying input torque. Considering the in-phase configuration as the base system, the phase angle is shifted by 25%, 50%, 75% and 100% with respect to the maximum twist angle of the cardan shaft that occurs at subcritical speed in in-phase configuration. The responses of the twist angle and the output speed are plotted against time.

3.1 Effect of Phase Angle on Sommerfeld Effect Under Constant Input Torque

Under the condition that $T_{in} = 474\ Nm$, the results of the numerical simulation, as shown in Figure 3, show an average output speed of 94.7 rad/s, reaching a maximum twist of 0.38 rad and remaining constant thereafter. However, the estimated rotational speed of the output shaft is 158 rad/s. This means a deviation of about 40% between the estimated and the simulated values. The manifestation of the Sommerfeld effect can be observed in the increase of the torsional vibration amplitude and the occurrence of the captured output speed. The speed capture occurred at about half the natural frequency of the system, which was found to be a subcritical speed range. During the speed capture, the input torque was used to amplify the torsional vibration instead of increasing the output shaft speed.

The Sommerfeld effect is expected to be attenuated by setting the phase angle to a specific amount relative to the maximum twist that occurs in the in-phase configuration. Table 2 shows the tabulated phase angle values, where the value of δ represents a shifted angular position of the yoke of the output shaft and is derived from Equation 4.

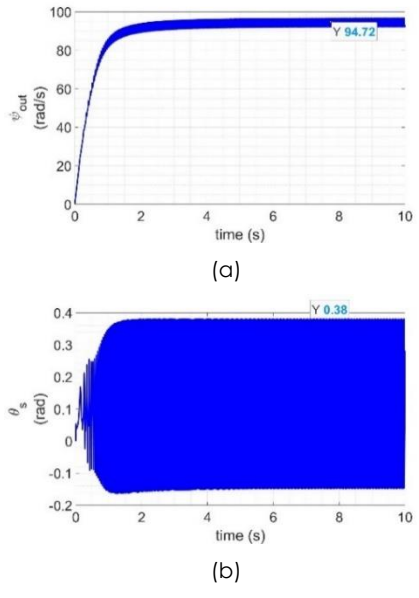

Figure 3 Time response of the system at 474 Nm and in-phase configuration: (a) output speed, (b) torsional vibration

Table 2 Tabulated phase angle for 474 Nm

Input torque (Nm)	Maximum twist (rad)	Case	α (rad)	δ (rad)
474	0.38	A (25%)	0.1	0.05
		B (50%)	0.19	0.11
		C (75%)	0.29	0.16
		D (100%)	0.38	0.22

When the phase angle is set to 25%, the average output speed shown in Figure 4 has escaped the speed capture in the subcritical speed region and smoothly increased to the estimated speed of 157.6 rad/s, then decreased to a steady average output speed of 150 rad/s, or 5% deviation compared to the estimated output speed. The torsional vibration result also shows a reduction in amplitude at the subcritical speed from 0.38 rad to 0.22 rad, or a reduction of about 26%. In the cases where the speed capture is bypassed, there is a reduction in the power dissipation of the drive due to the reduced torsional vibrations, so that the excess power can be used to accelerate the output shaft. Although there is a downward jump after the estimated output speed is reached, the amplitude of the torsional vibrations of 0.34 rad is still lower than the speed recorded in the in-phase configuration. The occurrence of downward jumps and the increase in torsional amplitude are due to the approach to the natural frequency of the system.

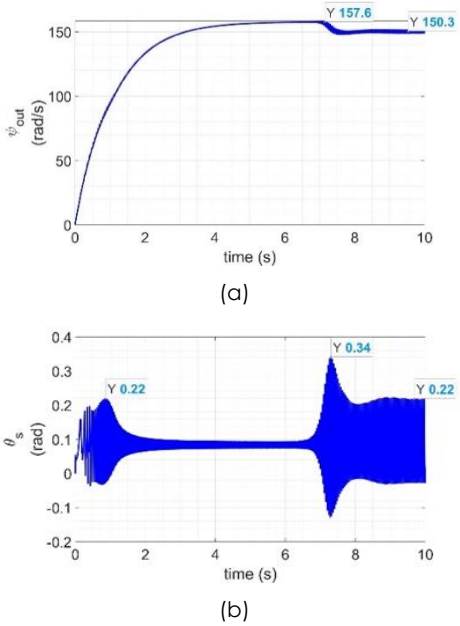

Figure 4 Time response of the system at 474 Nm and 25% phase angle: (a) output speed, (b) torsional vibration

When the phase angle is increased to 50%, as shown in Figure 5, the simulated average initial velocity increases to 153 rad/s, followed by a sudden decrease to 143 rad/s. Compared to the estimated output speed, the estimation error is about 15 rad/s or 10%. Furthermore, the system managed to escape speed capture while reducing the amplitude of torsional vibrations at subcritical and critical speeds to 0.15 rad and 0.27 rad, respectively.

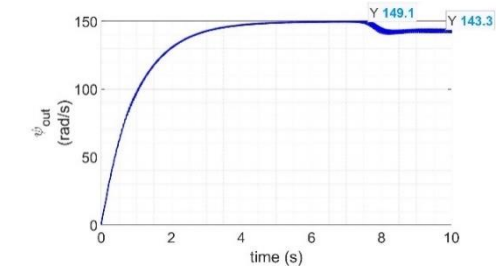

(a)

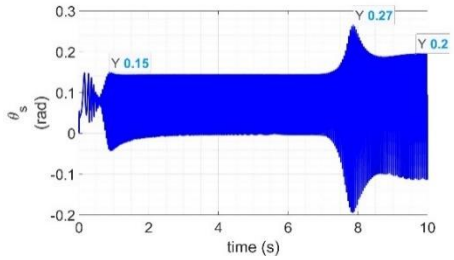

(b)

Figure 5 Time response of the system at 474 Nm and 50% phase angle: (a) output speed, (b) torsional vibration

As can be seen in Figure 6, the average output speed reaches only 123 rad/s when the phase angle is set to 75%. The observed deviation from the estimated rotational speed is about 35 rad/s, which corresponds to a discrepancy of 22%. The amplitudes of the torsional vibrations show fluctuations from 0.26 radian to -0.23 radian. When the phase angle is increased to 100%, the average output speed is recorded at 70 rad/s, as shown in Figure 7. The observed deviation from the estimated rotational speed is about 88 rad/s, which corresponds to a relative discrepancy of 55%. The maximum amplitudes of the torsional vibrations have reached 0.34 radians as recorded in the in-phase configuration. The increased amplitude variation is due to the relationship between the kinematics of the universal joint and the phase angle, which is directly proportional.

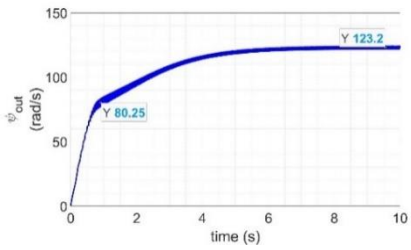

(a)

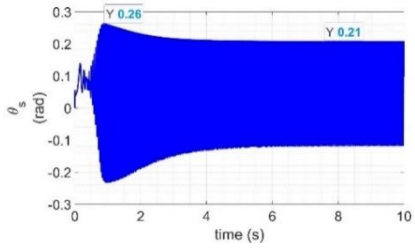

(b)

Figure 6 Time response of the system at 474 Nm and 75% phase angle: (a) output speed, (b) torsional vibration

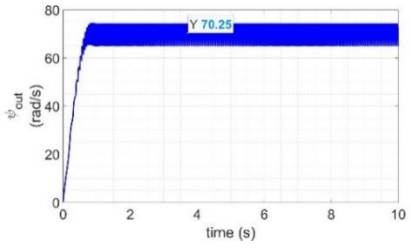

(a)

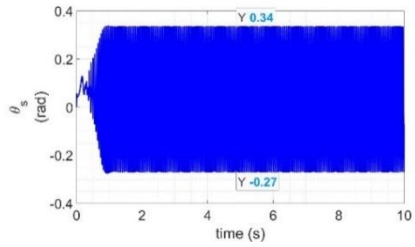

(b)

Figure 7 Time response of the system at 474 Nm and 100% phase angle: (a) output speed, (b) torsional vibration

Results of simulation shown in Figure 4 to Figure 7 have indicated that the system achieves a higher average output speed when operating with a phase angle between 25% and 50%. It is therefore necessary to carry out further investigations with different input torques for these two values of the phase angle. The next set of simulation results relates to the input torque increased to 765 Nm, with an estimated average output speed of 255 rad/s. In the in-phase configuration, after reaching a subcritical speed, the output speed increases to 224 rad/s at a maximum twist of 0.56 rad, before dropping to an average speed of 168 rad/s at a twist of 0.6 rad (see Figure 8).

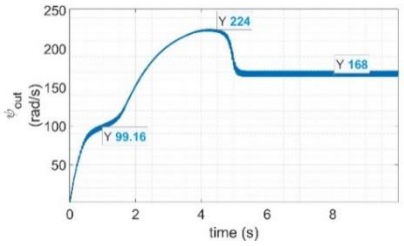

(a)

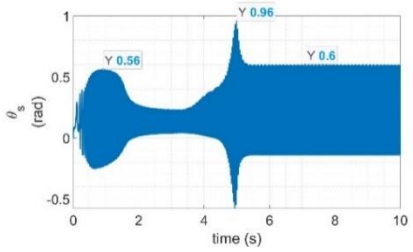

(b)

Figure 8 Time response of the driveline at 765 Nm and in-phase configuration: (a) output speed, (b) torsional vibration

When the phase angle is set to 25%, as shown in Figure 9, no Sommerfeld effect is observed and the output speed increases smoothly to the estimated output speed, 255 rad/s, reducing the vibration amplitude by about 41% at subcritical speed and 83% at critical speed compared to the in-phase configuration. Torsional vibrations are also better attenuated as the average output speed is approached.

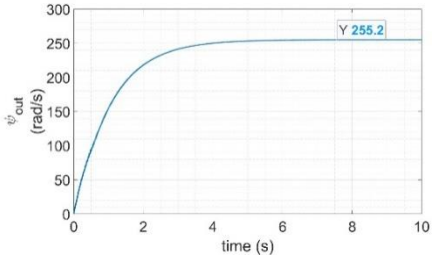

(a)

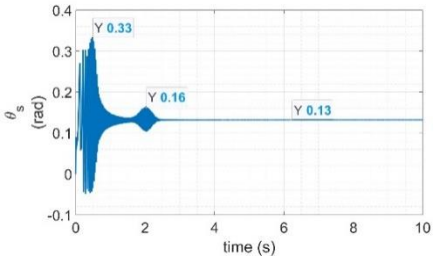

(b)

Figure 9 Time response of the system at 765 Nm and 25% phase angle: (a) output speed, (b) torsional vibration

When the phase angle is increased to 50%, as shown in Figure 10, a short duration of speed capture is observed at 208 rad/s. The average output speed reaches only 236 rad/s, which is lower than average output speed while in the phase angle of 25%, even when the torsional vibration amplitudes are reduced at subcritical speed. Compared to the phase angle of 25%, the amplitude of the continuos vibration is 38% larger at 0.21 rad.

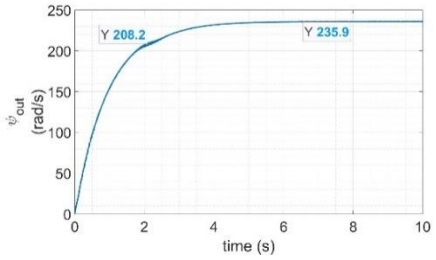

(a)

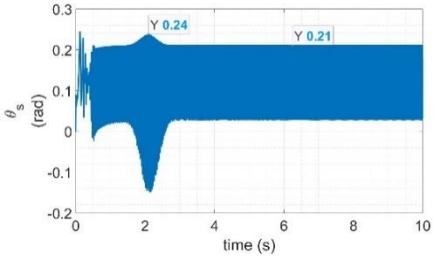

(b)

Figure 10 Time response of the system at 765 Nm and 50% phase angle: (a) output speed, (b) torsional vibration

3.2 Effect of Phase Angle on Sommerfeld Effect Under Gradually Varying Input Torque

In the normal Sommerfeld effect, upward jumps in speed are observed during the rotor coast up phase, while downward jumps are observed during the rotor coast down phase. Furthermore, these jumps occur at different speeds. To determine the effectiveness of the phase angle in suppressing this phenomenon within the power system, the input torque is systematically varied in a quasi-static manner, following a trapezoidal profile. The torque is gradually increased at a rate of 1 Nm/s until it reaches its maximum value of 480 Nm. The estimated output speed at 480 Nm is 160 rad/s. The maximum torque remains constant for 120 seconds and is then reduced to zero at a rate of 1 Nm/s. The results shown in Figure 11 show two cases of speed fluctuation, one characterized by upward jumps and the other by a downward jump. Both upward and downward jumps are observed in the subcritical speed range. The upward jump occurred between rotational speeds of about 99 rad/s and 149 rad/s. The downward jump is observed when the average output speed drops from about 110 rad/s to 88 rad/s during the rotor coast down process.

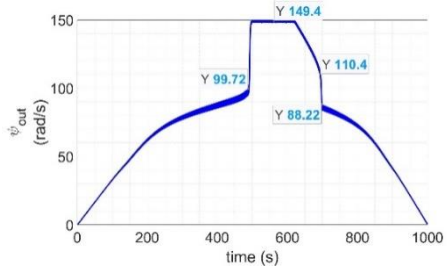

(a)

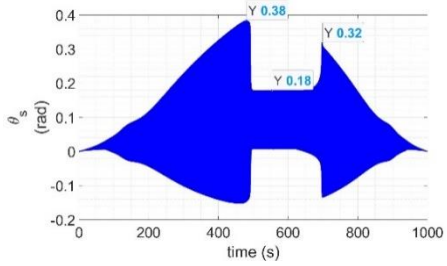

(b)

Figure 11 Time response of the system at gradually changing input torque and in-phase configuration: (a) output speed, (b) torsional vibration

At a phase angle of 25%, both the upward and downward jumps are suppressed, as shown in Figure 12. A higher output speed, 151 rad/s is achieved with a maximum torsional amplitude is reduced from 0.38 rad to 0.23 rad. The observed deviation from the estimated output speed is about 9 rad/s, which corresponds to a discrepancy of 5%. With a phase angle of 50%, as shown in Figure 13, the Sommerfeld effect is observed in the subcritical speed range during the coast up and coast down phase. The output speed is reduced to 143.3 rad/s, which is 10% lower than the estimated output speed. The Sommerfeld effect results in fluctuation of vibration amplitude at subcritical ranging from 0.18 rad to -0.15 rad. The vibration amplitude at maximum torque also exhibits oscillations ranging between 0.2 radians and -0.1 rad. The increased fluctuations in vibration amplitude indicate that the system experiences the Sommerfeld effect.

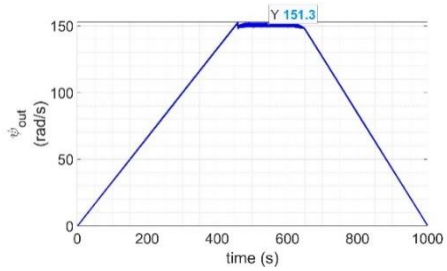

(a)

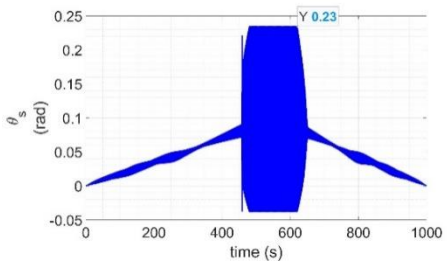

(b)

Figure 12 Time response of the system at gradually changing input torque and 25% phase angle: (a) output speed, (b) torsional vibration

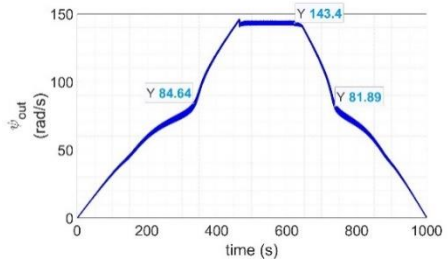

(a)

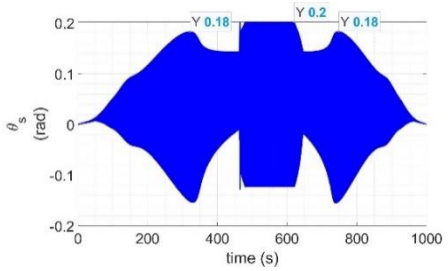

(b)

Figure 13 Time response of the system at gradually changing input torque and 50% phase angle: (a) output speed, (b) torsional vibration

4.0 CONCLUSION

In this study, the Sommerfeld effect in a power transmission system with a cardan shaft was analyzed using the numerical method. The model and analysis developed in this study incorporate the phase angle effect into the governing equation as well as the full kinematics relationship of the universal joint. The responses of the system were simulated for scenarios with constant and gradually varying input torque. While in-phase configuration, the Sommerfeld effect occurred in two regions. One region was near half the natural frequency, while the other was observed at the natural frequency. These regions were classified as subcritical and critical speed regions, respectively. The suppression method of the Sommerfeld effect was by compensating the phase angle between the two universal joints of the cardan shaft. The phase angle was set to 25%, 50%, 75%, and 100% of the maximum twist angle observed in the subcritical speed range of

the in-phase configuration to suppress the Sommerfeld effect. The results have shown that a phase angle of 25% has suppressed the Sommerfeld effect, resulting in a 5% deviation in the output speed from the expected value for both input torque scenarios. This study provides evidence of the impact of phase angle modification on suppressing the Sommerfeld effect and system vibrations. The finding emphasizes the importance of considering these factors during the design and motivates future studies to validate the findings through experimental work before actual rotating machinery implementation.

Conflicts of Interest

The author(s) declare(s) that there is no conflict of interest regarding the publication of this paper.

Acknowledgement

This work was sponsored by the Malaysian Ministry of Higher Education under the Hadiah Latihan Persekutuan (HLP) scheme.

References

[1] Ding, J., Lin, J., Yu, S. 2015. Dynamic Unbalance Detection of Cardan Shaft in High-speed Train Applying Double Decomposition and Double Reconstruction Method. *Measurement.* 73: 111-120.

[2] Yi, C., Lin, J., Ruan, T., Li, Y. 2015. Real Time Cardan Shaft State Estimation of High-speed Train based on Ensemble Empirical Mode Decomposition. *Shock and Vibration.* https://doi.org/10.1155/2015/912483.

[3] Golafshan, R., Dascaliuc, C., Jacobs, G., Roth, D., Berroth, J., Neumann, S. 2021. Damage Diagnosis of Cardan Shafts in Mobile Mining Machines using Vibration Analysis. *IOP Conference Series: Materials Science and Engineering.* 1097: 012019.

[4] Hu, Y., Zhang, B., Tan, A. C. 2020. Acceleration Signal with DTCWPT and Novel Optimize SNR Index for Diagnosis of Misaligned Cardan Shaft in High-speed Train. *Mechanical Systems and Signal Processing.* 140: 106723.

[5] Huang, Q., Yan, X., Wang, Y., Zhang, C., Wang, Z. 2017. Numerical Modeling and Experimental Analysis on Coupled Torsional-longitudinal Vibrations of a Ship's Propeller Shaft. *Ocean Engineering.* 136: 272-282.

[6] Hu, Y., Lin, J., Tan, A. C. 2019. Failure Analysis of Gearbox in CRH High-speed Train. *Engineering Failure Analysis.* 105: 110-126.

[7] Liu, J. S. P., Remisoski, N., Iqbal, J., Egenolf, R. 2017. CAE Predictions for Cardan Joint Induced Driveline NVH. SAE Technical Papers. https://doi.org/10.4271/2017-01-1136.

[8] Kato, M., Ota, H. 1990. Lateral Excitation of a Rotating Shaft Driven by a Universal Joint with Friction. *Journal of Vibration and Acoustics, Transactions of the ASME* 112: 298-303.

[9] Han, H. S., Lee, K. H. 2019. Experimental Verification for Lateral-torsional Coupled Vibration of the Propulsion Shaft System in a Ship. *Engineering Failure Analysis.* 104: 758-771.

[10] Hu, Y., Chit Tan, A., Liang, C., Li, Y. 2021. Failure Analysis of Fractured Motor Bolts in High-speed Train Due to Cardan Shaft Misalignment. *Engineering Failure Analysis.* 122: 105246.

[11] Zheng, Z., Lin, J., Hu, Y., Zhou, Q., Yi, C. 2022. Dynamic Unbalance Identification and Quantitative Diagnosis of Cardan Shaft in High-speed Train based on Improved TQWT-RBFNN-NSGA-II Method. *Eng Fail Anal*. https://doi.org/10.1016/j.engfailanal.2022.106226.

[12] Tchomeni, B. X., Alugongo, A. 2020. Theoretical and Experimental Analysis of an Unbalanced and Cracked Cardan Shaft in the Vicinity of the Critical Speed. *Mathematical Models in Engineering.* 6: 34-49.

[13] An, K., Wang, W. 2017. Transmission Performance and Fault Analysis of a Vehicle Universal Joint. *Advances in Mechanical Engineering*. https://doi.org/10.1177/1687814017707478.

[14] Fischer, I. S., Paul, R. N. 1991. Kinematic Displacement Analysis of a Double-cardan-joint Driveline. *Journal of Mechanical Design, Transactions of the ASME.* 113: 263-271.

[15] Wu, G., Shi, W., Chen, Z. 2013. The Effect of Multi-universal Coupling Phase on Torsional Vibration of Drive Shaft and Vibration of Vehicle. SAE Technical Paper.

[16] Sundar Dasgupta, S. 2022. Dynamics of a Non-Ideal Gyroscopic Rotor System with Translational-Rotational Coupling Effect of External and Internal Damping. *Mechanics of Solids.* 57: 604-616.

[17] Bharti, S. K., Samantaray, A. K. 2021. Resonant Capture and Sommerfeld Effect due to Torsional Vibrations in a Double Cardan Joint Driveline. *Communications in Nonlinear Science and Numerical Simulation.* 97: 105728.

[18] Yao, W., DeSmidt, H. 2021. Nonlinear Coupled Torsion/Lateral Vibration and Sommerfeld Behavior in a Double U-Joint Driveshaft. *Journal of Vibration and Acoustics.* 143: 1-15.

[19] Sinha, A., Bharti, S. K., Samantaray, A. K., Bhattacharyya, R. 2020. Sommerfeld Effect in a Single-DOF System with base Excitation from Motor Driven Mechanism. *Mech Mach Theory*. https://doi.org/10.1016/j.mechmachtheory.2020.103808

[20] Sinha, A., Samantaray, A. K. 2023. Escape through Parametric Instabilities in a Non-ideal Motor Driven Geared Rotor Shaft Driveline. *Mechanism and Machine Theory*. 180: 105166.

[21] Bharti, S. K., Sinha, A., Samantaray, A. K., Bhattacharyya, R. 2021. Dynamics of a Rotor Shaft Driven by a Non-ideal Source through a Universal Joint. *Journal of Sound and Vibration.* 499: 115992.

[22] Jha, A. K., Dasgupta, S. S. 2020. Suppression of Sommerfeld Effect in a Non-ideal Discrete Rotor System with Fractional Order External Damping. *European Journal of Mechanics, A/Solids.* https://doi.org/10.1016/j.euromechsol.2019.103873.

[23] Jha, A. K., Dasgupta, S. S. 2019. Attenuation of Sommerfeld Effect in an Internally Damped Eccentric Shaft-disk System via Active Magnetic Bearings. *Meccanica.* 54: 311-320.

[24] SoltanRezaee, M., Ghazavi, M. R., Najafi, A., Rahmanian, S. 2018. Stability of a Multi-body Driveshaft System Excited through U-joints. *Meccanica.* 53: 1167-1183.

[25] Zají˜ Cek, M., Dupal, J. 2014. Analytic Solution of Simplified Cardan's Shaft Model.

[26] Schmelz, F., Seherr-Thoss, CH-C., Aucktor, E. 1992. Universal Joints and Driveshafts. Universal Joints and Driveshafts. https://doi.org/10.1007/978-3-662-02746-2.

[27] Chaban, A., Łukasik, Z., Popenda, A., Szafraniec, A. 2021. Mathematical Modelling of Transient Processes in an Asynchronous Drive with a Long Shaft Including Cardan Joints. *Energies (Basel)*. https://doi.org/10.3390/en14185692.

[28] Xia, Y., Pang, J., Yang, L., Zhao, Q., Yang, X. 2019. Nonlinear Numerical and Experimental Study on the

Second-order Torsional and Lateral Vibration of Driveline System Connected by Cardan Joint. *JVC/Journal of Vibration and Control.* https://doi.org/10.1177/1077546319889846.

[29] Murawski, L., Dereszewski, M. 2020. Theoretical and Practical Backgrounds of Monitoring System of Ship Power Transmission Systems' Torsional Vibration. *Journal of Marine Science and Technology (Japan)*. 25: 272-284.